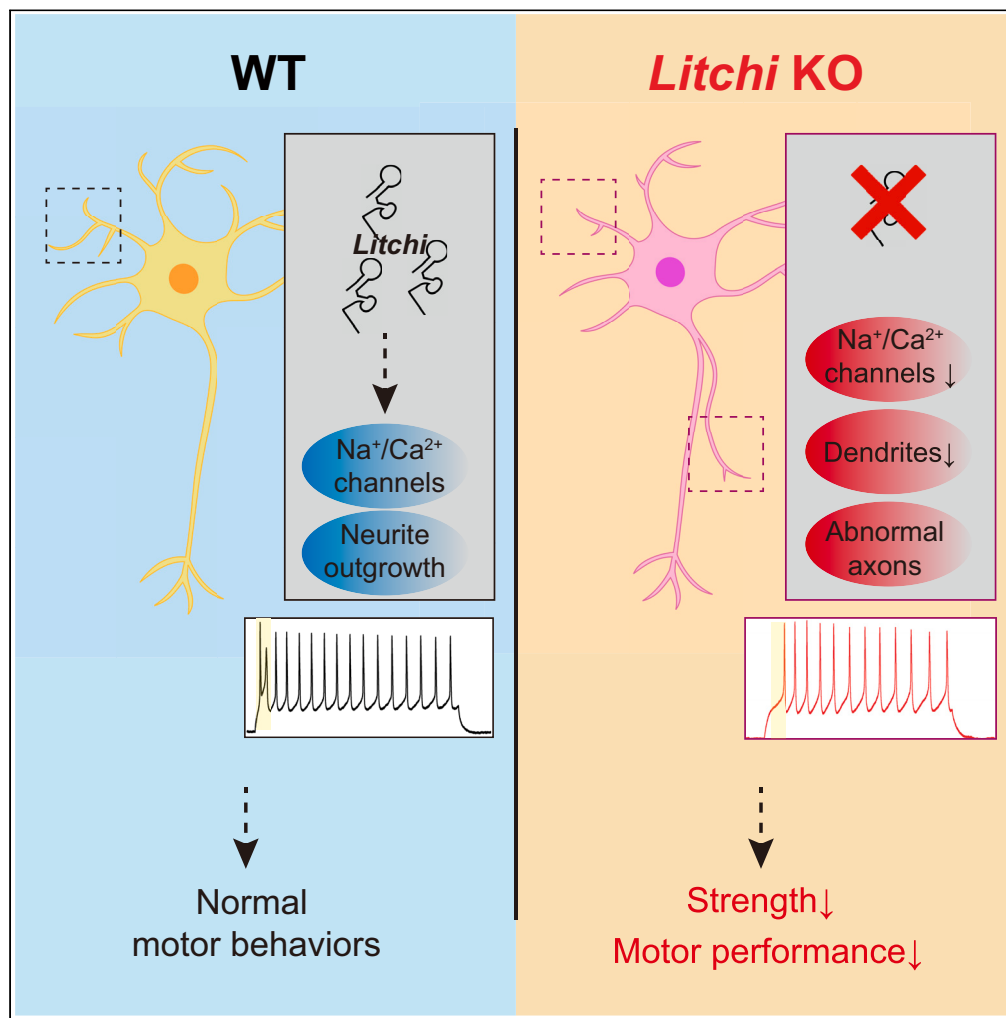


Article

LncRNA *Litchi* is a regulator for harmonizing maturity and resilient functionality in spinal motor neurons



Ho-Chiang Hsu,
Sheng-Ping Hsu,
Fang-Yu Hsu, Mien
Chang, Jun-An
Chen

jac2210@gate.sinica.edu.tw

Highlights

Litchi, a postmitotic MN-specific lncRNA, is located near the *Chat* genome locus

Deletion of *Litchi* impairs motor neuron dendritic complexity and axonal growth

Litchi-KO ESC ~ MNs show altered action potential patterns

The *Litchi*-KO mice exhibit impaired motor skills and muscle weakness

Hsu et al., iScience 27, 109207
March 15, 2024 © 2024 The Author(s).
<https://doi.org/10.1016/j.isci.2024.109207>



Article

LncRNA *Litchi* is a regulator for harmonizing maturity and resilient functionality in spinal motor neuronsHo-Chiang Hsu,^{1,2} Sheng-Ping Hsu,¹ Fang-Yu Hsu,^{1,4} Mien Chang,¹ and Jun-An Chen^{1,2,3,4,5,*}

SUMMARY

Long noncoding RNAs (lncRNAs) play pivotal roles in modulating gene expression during development and disease. Despite their high expression in the central nervous system (CNS), understanding the precise physiological functions of CNS-associated lncRNAs has been challenging, largely due to the *in vitro*-centric nature of studies in this field. Here, utilizing mouse embryonic stem cell (ESC)-derived motor neurons (MNs), we identified an unexplored MN-specific lncRNA, *Litchi* (Long Intergenic RNAs in *Chat* Intron). By employing an "exon-only" deletion strategy in ESCs and a mouse model, we reveal that *Litchi* deletion profoundly impacts MN dendritic complexity, axonal growth, and altered action potential patterns. Mechanistically, voltage-gated channels and neurite growth-related genes exhibited heightened sensitivity to *Litchi* deletion. Our *Litchi*-knockout mouse model displayed compromised motor behaviors and reduced muscle strength, highlighting *Litchi*'s critical role in motor function. This study unveils an underappreciated function of lncRNAs in orchestrating MN maturation and maintaining robust electrophysiological properties.

INTRODUCTION

Long non-coding RNAs (lncRNAs) represent a group of non-coding RNAs larger than 500 nucleotides with a lack of substantial peptide-coding capacity. Generally, lncRNA activity can be characterized based on their distributions at subcellular levels.^{1–3} For instance, in the nucleus, chromatin-associated lncRNAs that employ *cis* regulatory mechanisms are often tethered to their own gene loci, with this proximity facilitating the modulation of neighboring gene expression via the recruitment of transcriptional regulators or epigenetic complexes to modulate local transcription.^{4,5} Conversely, other lncRNAs operating in *trans* can influence distant loci to orchestrate gene regulatory functions.^{6,7} In the cytoplasm, lncRNAs can engage in direct interactions with other RNA species or with RNA-binding proteins, culminating in diverse actions such as mRNA stabilization, translational regulation, or serving as microRNA sponges.⁸ Notably, many studies have underscored that lncRNAs tend to be expressed in a cell-type-specific manner, with hundreds of lncRNAs being expressed prevalently within the central nervous system (CNS). However, only dozens of them have been characterized, and only a few have emerged as significant regulators of neuronal cell fate determination, differentiation, and maturation.^{9–12} Accordingly, the functions of the majority of lncRNAs in the CNS remain obscure.

Throughout the course of CNS development, diverse neuronal subtypes undergo intricate processes of differentiation and maturation. The foundational stage of the CNS commences with neurulation, leading to the subsequent elaboration of the neural tube into the brain and spinal cord, with this process being orchestrated by a cascade of genes prompted by morphogenic cues.^{13,14} Within the ventral spinal cord, the morphogen sonic hedgehog operates as a pivotal determinant, instigating the activation of specific transcription factor (TF) genes via a gradient emanating from the notochord and the floor plate.^{15–17} This nuanced gradient delineates five distinct progenitor domains (p0-2, pMN, and p3), with the pMN domain serving as the precursor of post-mitotic motor neurons (MNs), ultimately shaping their emergence from the developmental milieu.¹⁷ MNs exert a central role as the primary neural entities extending beyond the confines of the spinal cord, orchestrating both respiratory and motor functions. MNs acquire specialized identities across distinct motor columns spanning the expanse of the spinal cord. The ensuing diversity within MN subpopulations is reflected in axonal arborization to a spectrum of muscle types. At the molecular level, the blueprint for MN differentiation and diversification hinges upon the orchestrated interplay of specific TFs, with each pool of diversified MNs establishing its identity according to unique combinations of those TFs.^{9,18} These TF configurations intricately shape both the distinctive differentiation trajectories of MNs and their precision-guided axonal pathfinding strategies. Consequently, the MNs within each discrete motor column intricately establish a finely tuned connection network with disparate muscle fibers, ensuring impeccable

¹Institute of Molecular Biology, Academia Sinica, Taipei 11529, Taiwan²Taiwan International Graduate Program in Interdisciplinary Neuroscience, National Cheng Kung University and Academia Sinica, Taipei, Taiwan³Neuroscience Program of Academia Sinica, Academia Sinica, Taipei, Taiwan⁴Genome and Systems Biology Degree Program, Academia Sinica and National Taiwan University, Taipei 10617, Taiwan⁵Lead contact

*Correspondence: jac2210@gate.sinica.edu.tw

<https://doi.org/10.1016/j.isci.2024.109207>

functional coordination. Although decades of research endeavors have shed light on the functional roles of TFs and how their intricate combinations govern the establishment of distinct MN subtype identity, this framework remains incompletely characterized due to the paucity of detail on how lncRNAs integrate with and contribute to this process.

Our group, together with several previous studies, has discerned a cohort of lncRNAs that undergo dynamic shifts in expression throughout the process of MN differentiation.^{7,19,20} However, fewer than a dozen of these lncRNAs have been functionally characterized. Here, we focus on a novel MN-enriched lncRNA termed *Litchi* (Long Intergenic RNAs in *Chat* intron), characterizing its activity by gain-of-function and loss-of-function studies. We reveal a significant influence of *Litchi* deletion on MN dendritic complexity and axonal growth, and report that *Litchi* overexpression elicits extraordinarily long neurites in interneurons. *Litchi* deletion elevates the sensitivity of voltage-gated channels and causes dysregulated expression of neurite growth-related genes, as evidenced by our electrophysiological analyses that demonstrate altered action potential patterns. Notably, our *Litchi*-knockout mouse model exhibits compromised motor behaviors and reduced strength force, reinforcing *Litchi*'s significant role in motor function. Overall, our study highlights the unappreciated role of lncRNAs in governing MN maturation and physiological function, shedding light on the broader regulatory relevance of lncRNAs to the homeostasis responsible for maintaining the health of mature neurons.

RESULTS

Litchi (*Gm2990*) is a novel motor neuron-enriched long noncoding RNAs

Although it is known that lncRNAs are involved in neural development and degeneration,¹² their roles during MN development remain relatively unexplored. Previously, to uncover novel lncRNAs that might be essential to MN development, we utilized *Mnx1::GFP* ESCs and systematically differentiated them into spinal MNs or interneurons (INs) by means of established protocols⁷ (Figure 1A). Here, we compared MN progenitors (pMNs, Day4) and differentiated MNs (*Mnx1::GFP^{on}* cells, Day7) to acquire a list of developmentally upregulated lncRNAs (Table S1). Notably, we acquired 49 lncRNA species that are enriched (fold-change >2) in Day7 *GFP^{on}* cells but not in Day4 pMNs. From this list, we identified several lncRNAs previously reported as being important in MN development, including *Meg3*.⁷ Next, we determined which lncRNAs are differentially expressed in *GFP^{on}* cells and cross-referenced that list against lncRNAs identified from differentiated INs (*Mnx1::GFP^{off}* cells, Day7), which revealed 31 Day7-enriched lncRNAs showing high-level expression in *GFP^{on}* cells but not in *GFP^{off}* cells (Table S1). Next, we focused on novel lncRNAs that had not been reported previously, which uncovered nine novel lncRNA candidates, and verified the specificity of these MN-associated lncRNAs (mnLnc) by quantitative PCR (qPCR) at Days 4, 5, and 6 (Figures 1B and 1C). We searched for *cis*-acting mnLnc candidates and uncovered three located near one or more genes expressed in MNs (Figures 1D, 1E, and S1A–S1D). One candidate in particular, *Gm2990*, caught our attention as not only did it appear to be MN-specific, but its genomic locus is near the *Chat* (*Choline acetyltransferase*) and *Slc18a3* (*Vacht*, *Vesicular acetylcholine transporter*) cholinergic locus, with both of these latter being important for MN function (Figure 1D). Upon discovering two annotated isoforms (201 and 202) of *Gm2990* through Ensembl (Figure 1D), we conducted qPCR analysis using specific primers to distinguish between these two isoforms. Our investigation revealed that *Gm2990-201* exhibits predominant expression over *Gm2990-202* (Figure S1E). Based on these significant findings, we have renamed *Gm2990-201* as *Litchi* (Long Intergenic RNAs in *Chat* intron), and characterize its functions in detail later in discussion.

Litchi is exclusively expressed in spinal motor neurons

To profile *Litchi* expression during spinal cord development, we analyzed several single-cell RNA sequencing (scRNA-seq) datasets to confirm if *Litchi* exhibits a cell-type-specific expression pattern in the embryonic spinal cord^{18,21,22} (Figures 2A and 2B). Among the different cell types in the spinal cord, we found that *Litchi* was mainly expressed in MNs, similar to cholinergic genes (*Chat*, *Slc18a3*, and *Slc5a7*) (Figure 2A), and with no preference for a particular MN subtype (Figure 2B). To confirm the scRNA-seq data, we collected two MN subtypes, including lateral motor column (LMC: *GFP^{on}/RFP^{on}*) and medial motor column (MMC: *GFP^{off}/RFP^{on}*) MNs, as well as non-MN cells (*GFP^{off}/RFP^{off}*), from three segments (brachial, thoracic, and lumbar) of the spinal cord of E13.5 *Foxp1::GFP; Mnx1::RFP* double reporter mice²³ for quantitative reverse-transcription polymerase chain reaction (qRT-PCR) analyses (Figures 2C and S2A). Both LMC- and MMC-associated MNs in all three segments displayed significantly enriched levels of *Litchi* compared to non-MN cells. Next, we performed *in situ* hybridization (ISH) on E13.5 spinal cords to uncover *Litchi*-expressing cell distributions. We found that *Litchi* is primarily located at the ventral marginal zone of the spinal cord (Figures 2D and 2E), though it was not detected at the medial ganglionic eminence of the embryonic brain, a presumptive region enriched for *Chat/Slc18a3*-positive striatal and basal forebrain cholinergic neurons (Figure 2F). Collectively, these data indicate that *Litchi* is expressed exclusively in post-mitotic MNs.

Litchi expression is sustained in adult motor neurons

Given that *Chat/Slc18a3* (*Vacht*) expression is maintained in MNs into adulthood, we also analyzed an adult mouse MN scRNA-seq data,²⁴ which revealed that *Litchi* is as well expressed in all mature cholinergic neurons (Figure S2B). To further investigate *Litchi/Slc18a3* expression patterns at a cellular resolution, we performed multiplex fluorescence-based *in situ* hybridization using an RNAscope on different developmental stages of the mouse spinal cord. *Litchi* was detected at E12.5 (Figures S2C and S2D). *Litchi* expression was still robust for postnatal (P2) and adult (P120) mice, albeit weaker than for embryonic stages (Figure S2C). Together, our results pointed out that *Litchi* expression is being sustained in MNs from embryonic through postnatal stages and into adulthood.

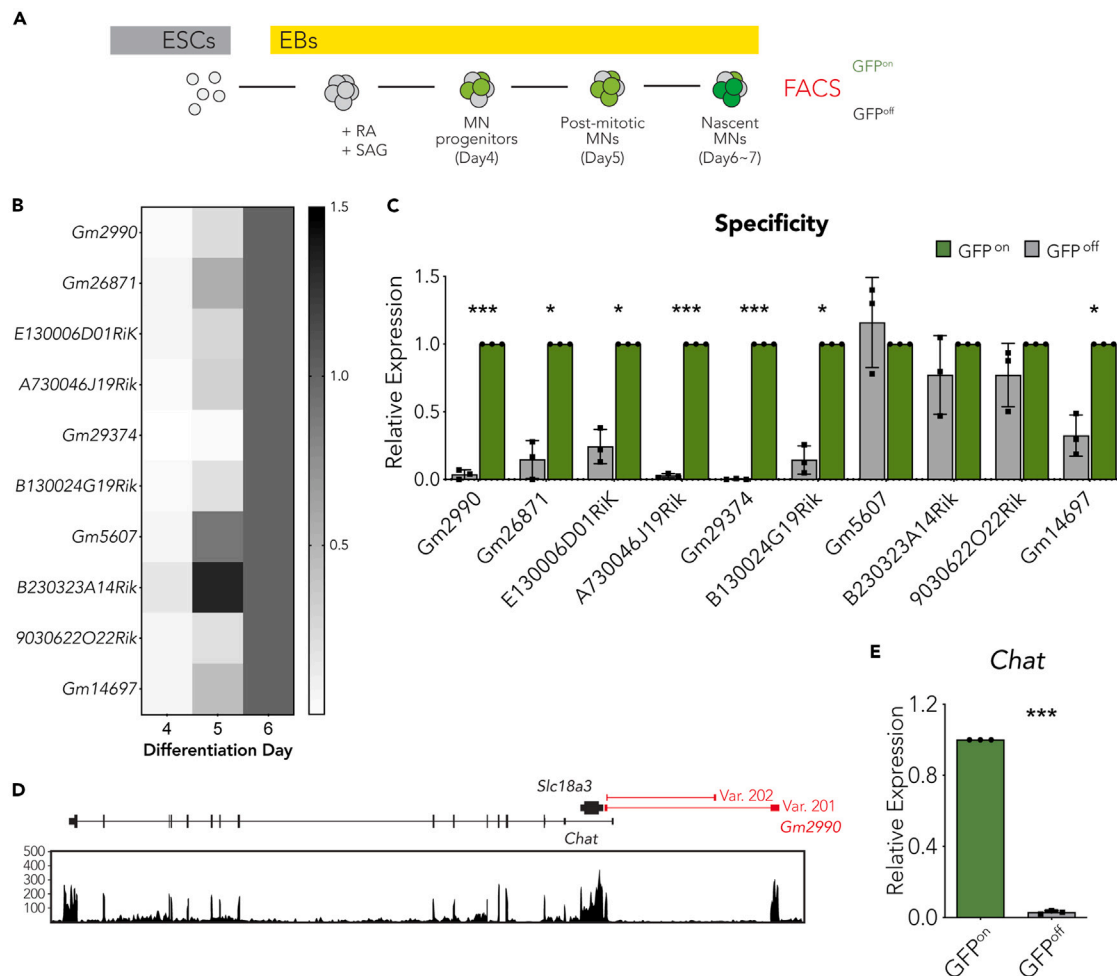


Figure 1. Investigation of motor neuron-enriched lncRNA candidates

(A) Schematic illustration of the MN differentiation process from mouse embryonic stem cells (ESCs). EBs: embryoid bodies. RA: retinoic acid. SAG: Smoothed agonist. MN: motor neuron.

(B) qPCR of MN-enriched lncRNAs from Day4~Day6 MNs. Gray-scale heatmap shows the relative expression level of each gene compared with the respective level in Day6 MNs. $N = 3$ independent experiments.

(C) qPCR of MN-enriched lncRNAs for GFP^{on} and GFP^{off} Day6 MNs. Statistics: unpaired t-test, $N = 3$ independent differentiation experiments. Data are presented as mean \pm SD. * $p < 0.05$, *** $p < 0.001$.

(D) Gene locus and expression levels of two variants (Var. 201 and Var. 202) of *Gm2990* and its neighboring genes *Chat* and *Slc18a3*.

(E) qPCR of *Chat* for GFP^{on} and GFP^{off} Day6 MNs. Statistics: unpaired t-test, $N = 3$ independent differentiation experiments. Data are presented as mean \pm SD. *** $p < 0.001$.

Characterization of *Litchi* knockout phenotypes in embryonic stem cell-derived motor neurons

To reveal the potential functions of *Litchi* in differentiated MNs, we used a CRISPR/Cas9-mediated approach to delete *Litchi* exons from *Mnx1::GFP* ESCs, allowing us to scrutinize resulting phenotypes during MN differentiation (Figure 3A). To avoid interference from the deletion of the first exon of *Chat*, we designed two sets of gRNAs to remove the two *Litchi* exons sequentially. We then confirmed the depleted expression of both *Litchi* exons from differentiated *Litchi*-KO MNs (Figure S3A). Surprisingly, expression levels of *Chat* and *Slc18a3* remained unaltered in the *Litchi*-KO ESC-derived MNs (Figure S3B), indicating that *Litchi* is not likely to function in *cis*. Next, we examined if *Litchi* impedes MN differentiation and observed that pMN (Olig2⁺) generation is not affected upon *Litchi* knockout (Figures S3C and S3D). However, we did detect a slight reduction in the number of Isl1/2⁺ cells among *Litchi*-KO MNs relative to Ctrl MNs (control: a *Litchi* heterozygous ESC line) (Figures S3C and S3E). This result is consistent with the expression of *Litchi* in postmitotic MNs but not in pMNs.

To further test if *Litchi* affects MN neurite morphology, we dissociated Ctrl and *Litchi*-KO embryoid bodies (EBs), harvested the same number of MNs, and seeded them on laminin-coated slides at Day5. Strikingly, within 6 h, we observed that *Litchi*-KO MNs already exhibited a pattern of shorter neurite growth than the Ctrl MNs (Figure S3F). This difference in neurite morphology peaked at 48 h after seeding (Day7)

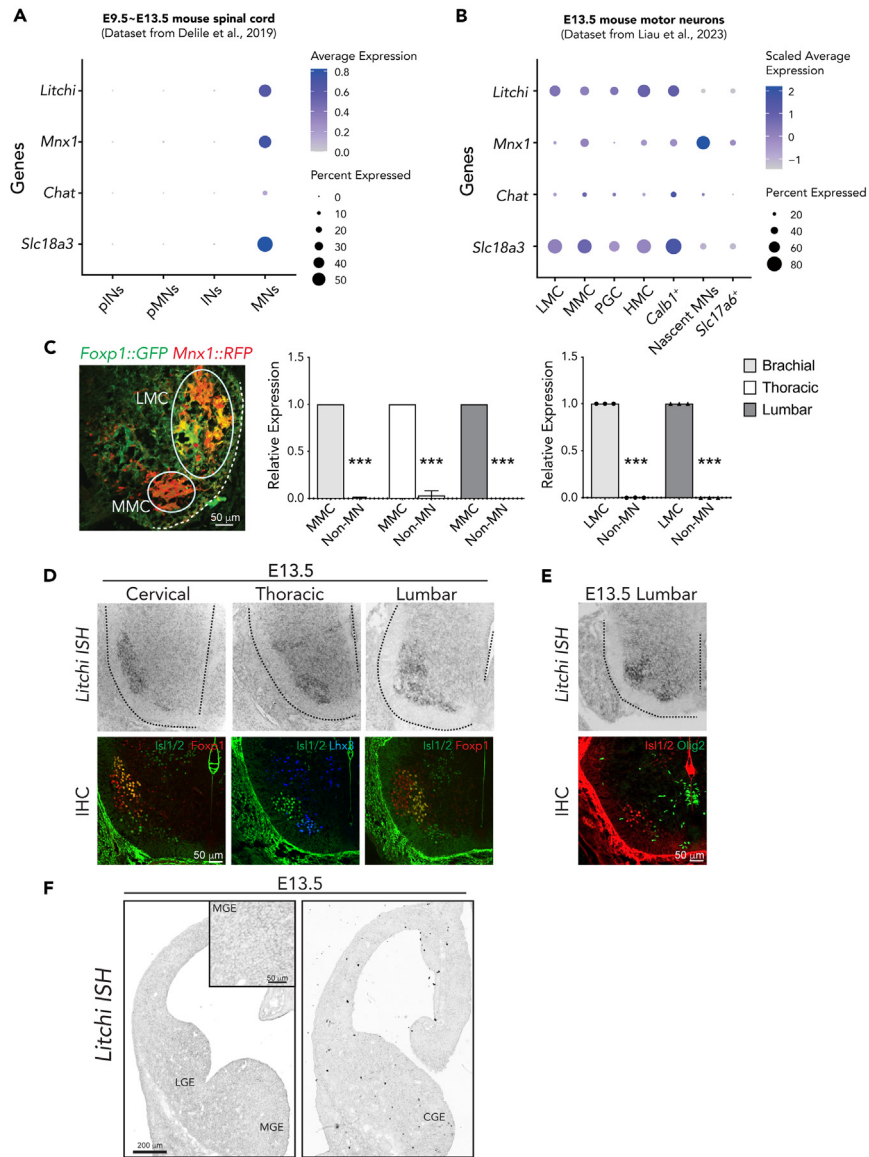


Figure 2. *Litchi* expression profile in the embryonic spinal cord

(A and B) Analysis of mouse embryonic spinal neuron scRNA-seq data from Delille et al., 2019 (A), and mouse embryonic *Mnx1::GFP^{on}* MN scRNA-seq data from Liao et al., 2022 (B). Color intensity reflects average expression level, whereas dot size represents the percentage of expressing cells among total analyzed cells. LMC: lateral motor column; MMC: medial motor column; PGC: preganglionic column; HMC: hypaxial motor column; Calb⁺: Calbindin positive neurons; Slc17a6⁺: Slc17a6 positive neurons.

(C) qPCR of sorted non-MN (*GFP^{off}*; *RFP^{off}*), MMC (*GFP^{off}*; *RFP^{on}*) and LMC (*GFP^{on}*; *RFP^{on}*) MNs. *Left*: Representative image of a *Foxp1::GFP*; *Mnx1::RFP* spinal cord section. *Middle*: relative *Litchi* expression level in brachial, thoracic and lumbar MMC MNs. *Right*: relative *Litchi* expression level in brachial and lumbar LMC MNs. Statistics: unpaired *t*-test, *N* = 3 independent experiments. Data are presented as mean \pm SD. ****p* < 0.001. Scale bar: 50 μ m.

(D) *Litchi* *in situ* hybridization (ISH) of E13.5 spinal cord and immunostaining of adjacent sections for *Isl1/2*, *Foxp1* and *Lhx3*. Scale bar: 50 μ m. Black dotted lines show the spinal cord central and ventral boundaries.

(E) ISH of *Litchi* in E13.5 lumbar spinal cord and immunostaining of adjacent sections for *Isl1/2* and *Olig2*. Scale bar: 50 μ m.

(F) ISH of *Litchi* in E13.5 mouse brain. LGE: lateral ganglionic eminence; MGE: medial ganglionic eminence; CGE: caudal ganglionic eminence. Scale bar: 200 μ m.

(Figure S3F). To determine the consequences of compromised neurite outgrowth upon *Litchi* knockout, we performed long-term MN culture with primary astrocytes to enable us to scrutinize neurite morphology (see STAR Methods for details). At Day6 of differentiation, we observed that both neurite length and branching number were significantly compromised in *Litchi*-KO MNs, whereas cell body area remained unaffected (Figures 3B and 3C). On Day10 of differentiation with astrocyte co-culture, MN neurites had further specified into dendrites and the axon (Figure 3D). By means of Sholl analysis (Figure 3E), we uncovered that *Litchi*-KO MNs displayed a tendency toward reduced dendrite

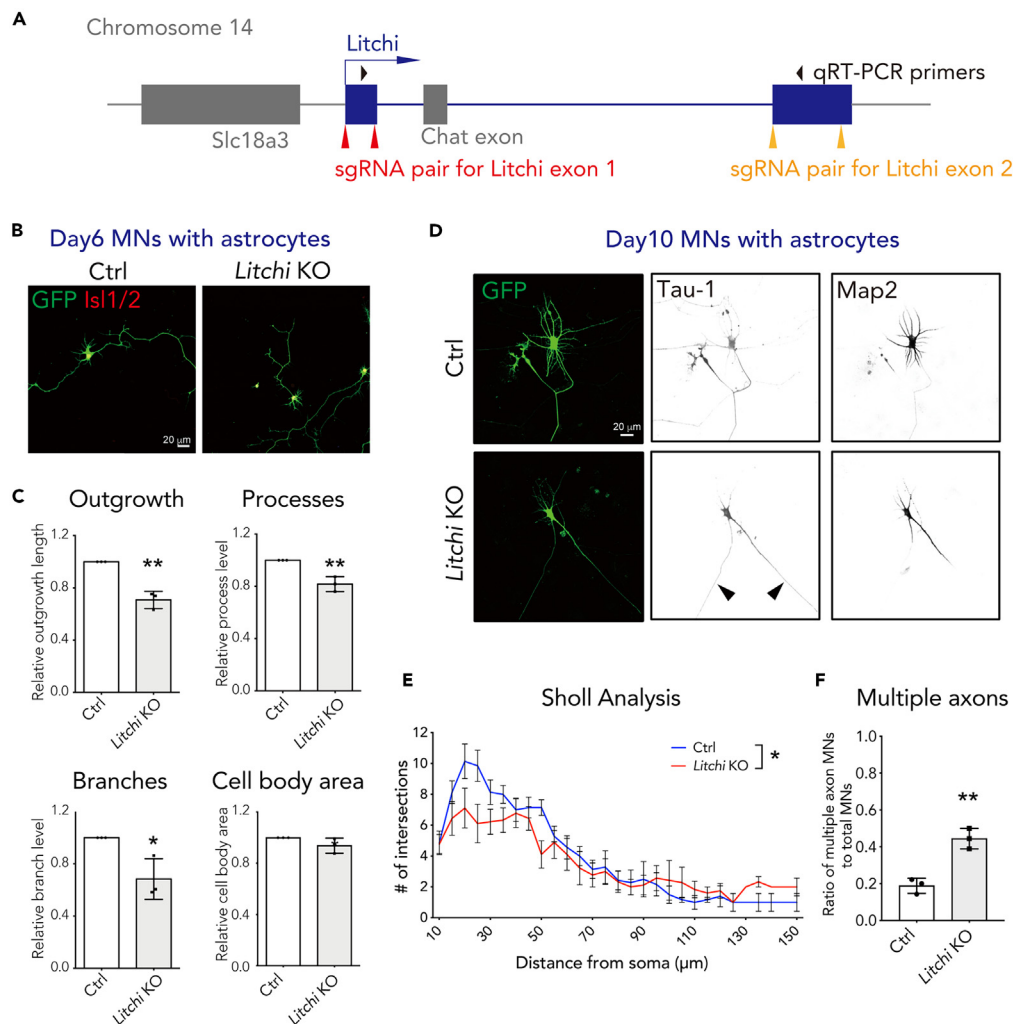


Figure 3. *Litchi*-KO ESC-derived MN phenotypes

(A) Design of CRISPR/Cas9-mediated deletions of the *Litchi* exons. Red arrowheads indicate the two sgRNAs for deleting *Litchi* exon 1; orange arrowheads indicate the sgRNAs for deleting *Litchi* exon 2. Black arrowheads indicate the location of the qPCR primers.

(B) Immunostainings for GFP and Isl1/2 in Day6 MNs co-cultured with astrocytes. Scale bar: 20 μm .

(C) Quantification of total neurite outgrowth, process number, branch number and cell body area of Day6 MNs. Statistics: unpaired t-test. * $p < 0.05$, ** $p < 0.01$. Specific significance: $p = 0.0016$ (outgrowth); 0.0052 (processes); 0.0245 (branches).

(D) Immunostainings for GFP, Tau-1 and Map2 in Day10 MN co-cultured with astrocytes. Scale bar: 20 μm .

(E) Sholl analysis of Map2⁺ dendrites. Statistics: two-way ANOVA. * $p < 0.05$. Specific significance: $p = 0.0131$.

(F) Quantification of the percentage of multiple Tau-1-positive axons. Statistics: unpaired t-test. ** $p < 0.01$. Specific significance: $p = 0.003$. $N = 3$ independent differentiation experiments.

complexity. Moreover, we also detected increased axon numbers for *Litchi*-KO MNs (Figure 3F). Thus, we postulate that *Litchi* might participate in the MN maturation process, particularly in determining dendrite complexity and axon development.

***Litchi* regulates the sensitivity of voltage-gated channels and neurite growth-related genes**

To investigate how *Litchi* affects neurite growth and axon development, we performed transcriptomics analysis on Ctrl and *Litchi*-KO ESC-derived MNs at differentiation Day7 (nascent MN stage) and Day9 after neurite growth (Figures 4A and 4B). As a result, we uncovered several gene pathways that are dysregulated upon *Litchi* knockout. At Day7, most ion transporter or channel-related genes were drastically down-regulated in the *Litchi*-KO MNs (as revealed by Gene Ontology, see STAR Methods for details). Moreover, the expression of genes related to the negative regulation of MN differentiation was also dampened, echoing the precocious maturation phenotype observed for *Litchi*-KO MNs. Conversely, the expression of genes linked to neurite and neuromuscular junction pathways—including ion channels, axon development, synapse formation, and neurite-related genes—were compromised on Day9, an outcome consistent with the morphological changes

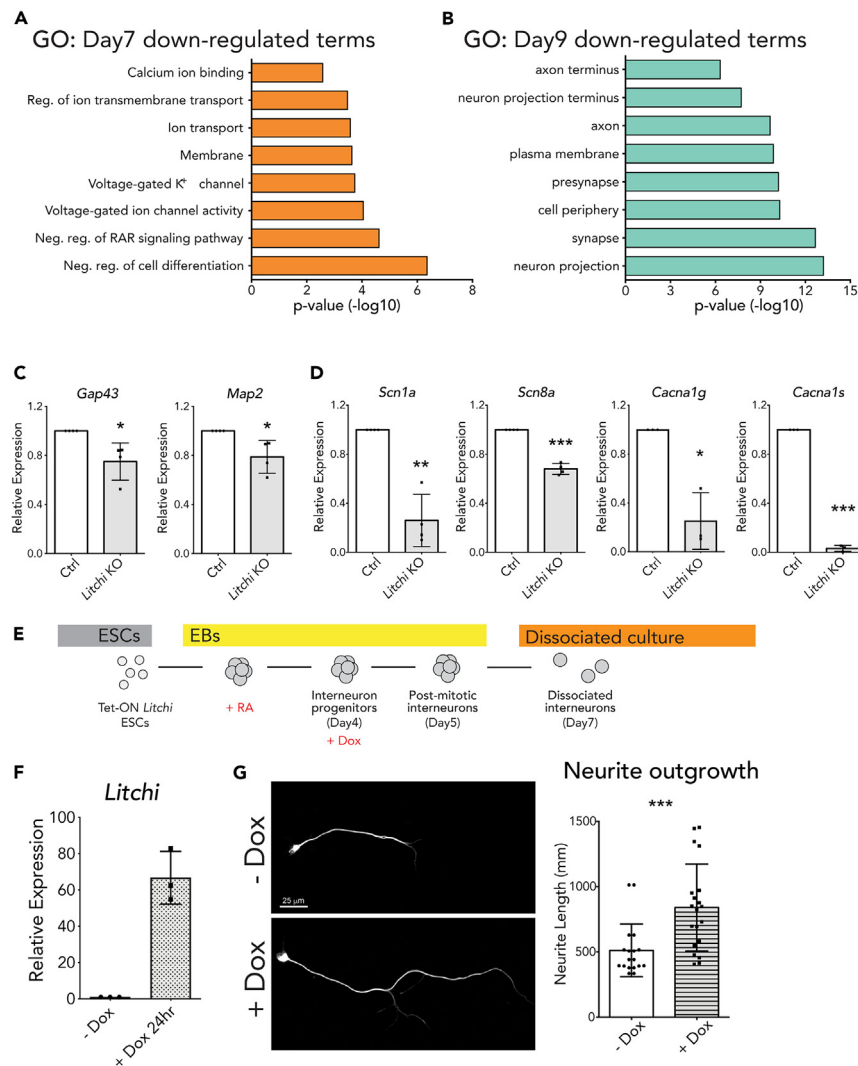


Figure 4. Gene ontology of *Litchi*-KO ESC-derived MNs and ectopic expression of *Litchi* in interneurons

(A and B) Gene ontology (GO) of downregulated genes from Day7 *Litchi*-KO embryoid bodies (EBs) (A) and Day9 *Litchi*-KO EBs (B).

(C) qPCR verification of downregulated neurite-related genes in Day9 *Litchi*-KO EBs. Statistics: unpaired t-test. Specific significance: $p = 0.0119$ (*Gap43*) and 0.0217 (*Map2*).

(D) qPCR verification of downregulated calcium and sodium channel genes in Day7 *Litchi*-KO EBs. Statistics: unpaired t-test. Specific significance: $p = 0.061$ (*Scn1a*), 0.0007 (*Scn8a*), 0.0304 (*Cacna1g*) and 0.0002 (*Cacna1s*).

(E) Schematic illustration of the interneuron (IN) differentiation process from Tet-on *Litchi* ESCs. Dox: doxycycline.

(F) *Litchi* induction efficiency: qPCR for *Litchi* was performed after adding doxycycline for 24 h.

(G) Left: immunostaining for anti-neurofilament on Day7 INs with or without doxycycline treatment. Scale bar: 25 μm. Right: quantification of neurite outgrowth length. Eighteen (-Dox) and 20 (+Dox) images from three independent experiments were subjected to analysis. Only monopolar or bipolar cells were counted. Statistics: unpaired t-test. Specific significance: $p = 0.0009$. $N > 3$ (for C, D and F) for independent differentiation experiments. * $p < 0.05$, ** $p < 0.01$, *** $p < 0.001$. Details of significance values are described in the respective panel legends. All data are presented as mean \pm SD.

displayed by *Litchi*-KO MNs. To verify these transcriptome profiling results, we collected Mnx1GFP Ctrl and *Litchi*-KO MNs by FACS for qPCR. We confirmed that the expression of two neurite-related genes (*Map2*, *Gap43*) was significantly reduced at Day7 (Figure 4C). Likewise, the expression of several genes encoding sodium and calcium channels (*Scn1a*, *Scn8a*, *Cacna1g*, and *Cacna1s*) was significantly reduced in the *Litchi*-KO MNs when compared to Ctrl (Figure 4D). Thus, *Litchi* appears to regulate dendrite complexity and axon development by mediating the expression of voltage-gated channels and neurite growth-related genes.

Furthermore, to confirm that *Litchi* can induce neurite outgrowth in neurons, we established Tet-ON *Litchi* mESCs to determine if *Litchi* overexpression in neurons could increase neurite growth during differentiation (Figure 4E). First, we confirmed that *Litchi* is robustly induced after doxycycline treatment in MNs (Figure 4F). Given that MNs exhibit a high expression level of *Litchi* and have already extended long axons,

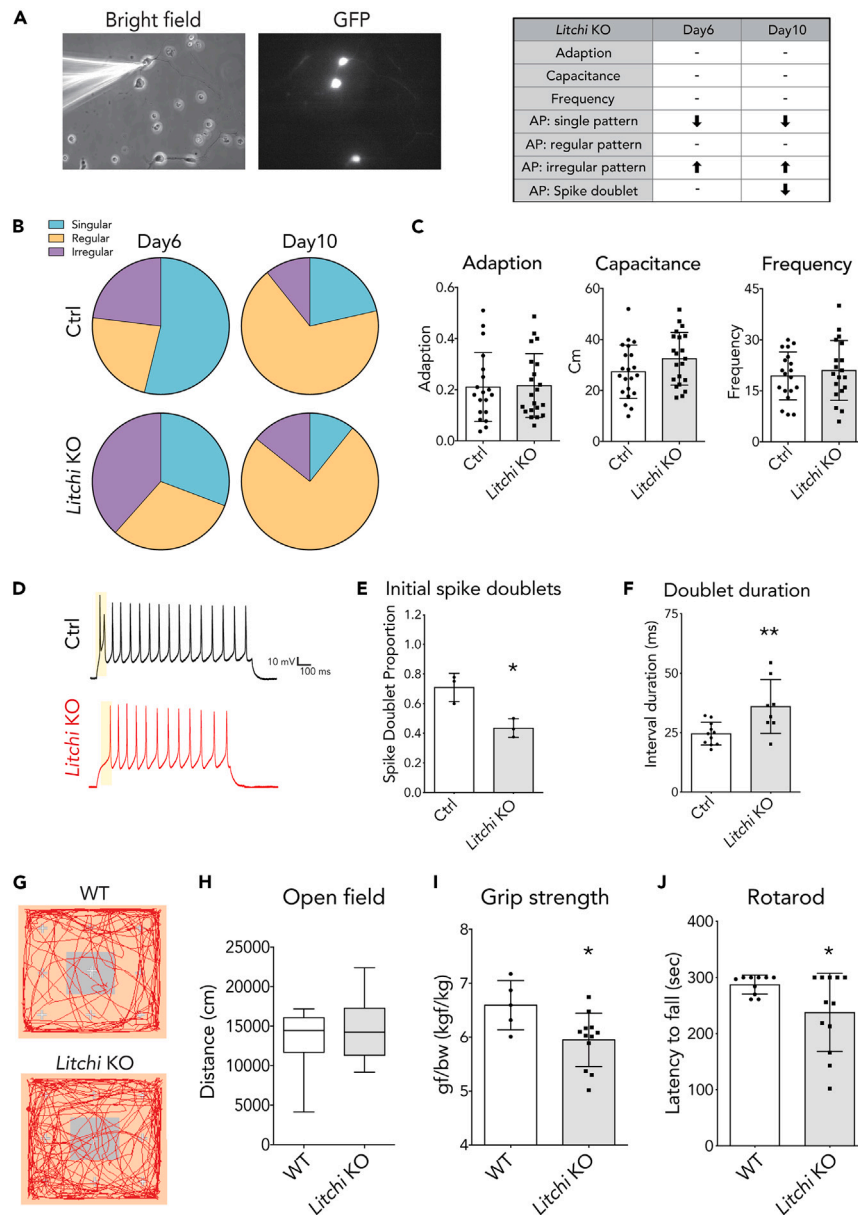


Figure 5. Electrophysiological and behavioral phenotypes of *Litchi*-KO model mice

(A) Representative images of the experimental process for patch clamping. A summary table of action potential (AP) results is presented at right.

(B) Proportion of singular, irregular and regular AP patterns in Day6 and Day10 ESC-derived MNs. At least 30 MNs for each group (Day6 Ctrl, Day6 *Litchi*-KO, Day10 Ctrl and Day10 *Litchi*-KO) were analyzed from three independent experiments.

(C) Analysis of the AP features of Day10 Ctrl and *Litchi*-KO MNs. At least 15 cells of each genotype (Ctrl and *Litchi*-KO) were measured from at least three independent experiments.

(D) Representative APs of Ctrl and *Litchi*-KO MNs.

(E) The proportion of initial spike doublets in Ctrl and *Litchi*-KO MNs. Statistics: unpaired t-test; * $p < 0.05$; specific significance: $p = 0.0141$. At least 15 cells of each genotype (Ctrl and *Litchi*-KO) were measured from at least three independent experiments.

(F) Duration of spike doublets. Duration was counted from the first peak to the second peak of MNs (Ctrl or *Litchi*-KO) generating spike doublets. Statistics: unpaired t-test; ** $p < 0.01$; specific significance: $p = 0.0077$. $N > 8$ MNs generating spike doublets of each genotype (Ctrl and *Litchi*-KO) were measured from at least three independent experiments.

(G) Representative open field recording of wild-type (WT) and *Litchi*-KO mice in the first 10 min.

(H) Quantification of total walking distance over 60 min. $N = 12$ (both WT and *Litchi*-KO) mice at the age of 1.5-month-old (mo). Data are presented as a box and whisker plot.

Figure 5. Continued

(I) Grip strength test. Force strength is normalized to the mouse body weight. $N = 5$ (WT) and 12 (*Litchi*-KO) 1.5-month mice. Statistics: unpaired t-test; $*p < 0.05$; specific significance: $p = 0.0382$.

(J) Latency-to-fall in a rotarod test for WT and *Litchi*-KO mice. The best performance of each mouse from three trials was recorded. $N = 12$ (both WT and *Litchi*-KO) 1.5-month mice. Statistics: unpaired t-test; $*p < 0.05$; specific significance: $p = 0.0409$. All bar chart data are presented as mean \pm SD.

we instead induced *Litchi* in ESC-derived interneurons, which do not express *Litchi* and have shorter axon lengths to test if *Litchi* is sufficient to ectopically induce neurite outgrowth in a non-MN context. Notably, we observed that ectopic *Litchi* expression elicited a dramatic increase in the neurite length of interneurons (Figure 4G). Taken together, these results indicate that *Litchi* is a novel MN-specific lncRNA that regulates the MN maturation process by controlling a set of neuronal-enriched genes, including a suite of ion channels. The *Litchi*-mediated MN maturation process is likely critical for MNs to exert robust physiological functions when they attain maturity.

***Litchi* knockout leads to aberrant motor neuron firing activity**

Our observation of compromised dendrite and axon development in *Litchi*-KO MNs prompted us to investigate potential impairments in MN physiology. We collected ESC-derived MNs from both Ctrl and *Litchi*-KO groups at Day6 and Day10 for whole-cell patch clamping to record action potentials (AP) (Figure 5A). Notably, the *Litchi*-KO MNs exhibited distinct patterns of AP spikes (single, irregular, and regular, Figure S4A) compared to Ctrl MNs. At Day6, Ctrl MNs predominantly displayed a single spike pattern, whereas *Litchi*-KO MNs presented a significant decrease in single spikes, resembling the pattern observed in mature Day10 MN. Moreover, *Litchi*-KO MNs at Day6 exhibited an increased occurrence of other spike patterns compared to Ctrl Day10 MN (Figure 5B). Although both Ctrl and *Litchi*-KO MNs showed elevated levels of non-single regular spikes on Day10, the latter displayed a higher tendency for irregular spikes compared to Ctrl at that stage (Figure 5B). These findings suggest that *Litchi* likely regulates the pace of MN maturation. Despite differentiating precociously at Day6, *Litchi*-KO MNs exhibited abnormal electrophysiology upon maturation at Day10. Further analysis of mature MNs at Day10 revealed that *Litchi*-KO MNs generated fewer doublet spikes upon stimulation compared to Ctrl MNs (Figures 5D, 5E, and S4B). Additionally, the duration of doublets was slightly increased in *Litchi*-KO MNs (Figure 5F). In summary, our study indicates that the absence of *Litchi* in MNs alters AP spike patterns, particularly eliciting a reduction in spike doublets. This alteration may potentially affect MN physiology and their ability to regulate muscle contractions.

***Litchi*-KO mice display muscle weakness and compromised resilient motor learning**

Given the prominent phenotype displayed by the *Litchi*-KO MNs, next we generated *Litchi*-KO mice using the same exon-only sequential deletion approach deployed for the ESC knockout line. First, we confirmed that *Litchi* expression was depleted from E12.5 spinal cords in the *Litchi*-KO mice compared to wild-type (WT) (Figure S5A). *Litchi*-KO mice were born in expected Mendelian ratios (data not shown), displayed a normal appearance, were viable after birth, and had a normal lifespan (Figures S5B and S5C). Then, we assessed if *Litchi* affects MN generation in the spinal cord. Through a series of immunostainings, we observed comparable numbers of pMNs (Olig2⁺), generic MNs (Isl1/2⁺), and MN subtypes (Lhx3⁺ and Foxp1⁺) between the WT and *Litchi*-KO embryos (Figures S5D–S5G). We then harvested the primary MNs from WT and *Litchi*-KO spinal MNs to examine their dendritic complexity. Remarkably, we observed a delay in the timing of neurite growth and compromised dendritic complexity in the primary MNs of the *Litchi*-KO mice (Figures S5H and S5I), recapitulating the phenotype of primary MN cultures from *Litchi*-KO ESC-derived MNs.

Adult *Litchi*-KO mice display muscle weakness

Given that many lncRNA knockout mouse lines only display prominent physiological defects or obvious phenotypes after stress or injury²⁵ and *Litchi* expression is sustained into adulthood, we reasoned that *Litchi*-KO mice might exhibit a conspicuous phenotype upon aging. To investigate if the MN abnormality elicited by *Litchi* knockout in cultured MNs leads to compromised motor skills in adult mice, we performed a series of behavioral tests to determine their motor abilities and skills. We detected no significant differences between WT and *Litchi*-KO mice in terms of general exploratory behavior, i.e., distance traveled in the open field test (Figures 5G and 5H). Notably, compared to WT mice, the *Litchi*-KO mice exhibited strikingly reduced performances in the grip strength force and rotarod tests (Figures 5I and 5J), indicating that motor and balance coordination were compromised upon *Litchi*-KO. These phenotypes are in agreement with the neurite shortening, abnormal axon morphology, and aberrant electrophysiology manifested in *Litchi*-KO MNs *in vitro* and *in vivo*.

DISCUSSION

In the present study, our primary objective was to investigate lncRNAs expressed within spinal MNs throughout the differentiation process by employing MNs derived from ESCs. Our endeavors led to the identification of nine distinct mnLnc candidates. To substantiate our findings, we cross-referenced these lncRNAs with prior research literature, which unveiled that none of them had been reported previously as having discernible roles as functional regulators in MNs or indeed any other neuronal cell types. This outcome highlights their potential unappreciated roles in MN differentiation and function, especially given that many cell-type-specific lncRNAs remain to be characterized, even in this era of the single cell atlas by which almost all types of neurons have been identified.^{18,24}

Litchi is expressed from early embryonic postmitotic MNs into adulthood. However, we noticed that its expression declined after the postnatal stage. This pattern is quite different from the steady and robust expression of *Chat* and *Slc18a3* throughout neuronal life. Strikingly,

when we deleted *Litchi*, levels of both *Chat* and *Slc18a3* remained largely unaffected, indicating that *Litchi* likely does not play a major *cis*-regulatory role by directly controlling these neighboring genes. Furthermore, in contrast to *Chat* and *Slc18a3*, *Litchi*-depleted mice do not exhibit postnatal lethality. Despite all three genes being proximal, their disparate functional roles prompt the intriguing question of whether a divergent regulatory element governs their precise expression dynamics in MNs. The answer to that question holds promise for illuminating novel regulatory mechanisms and thus warrants dedicated investigation in future. Moreover, although our transcriptomic analysis identified a suite of dysregulated genes upon *Litchi* knockout, it remains to be established if *Litchi* affects these genes directly. Further experiments using RNA pulldown assays or mass spectrometry-based ChIRP-MS to establish the *Litchi*-protein interactome might shed light on this issue.

Why does the impairment of *Litchi* in MNs give rise to the altered pattern of AP spikes? In particular, *Litchi*-KO MNs displayed a reduction in spike doublets, which might negatively impact MN physiology and consequently their ability to control muscle contractions. AP generation is impacted by several types of ion currents. Our transcriptomic data revealed that not only is the expression of neurite projection-linked genes downregulated in *Litchi*-KO MNs, but an important group of ion channel/transporting genes is similarly affected. Indeed, we found that several voltage-gated calcium and sodium channels were downregulated in the *Litchi*-KO MNs. Previous studies have shown that a reduction in intracellular sodium or voltage-gated sodium channels elicits a decline in AP spike doublets in the initial region of several types of stimulated neurons,^{26–28} with our data herein also revealing a similar pattern of reduced spike doublets in the *Litchi*-KO MNs. These results indicate that *Litchi* might affect several ion channel or transport genes. Moreover, a reduction in spike doublets has been correlated previously to muscle strength performance,^{29,30} and our motor behavior tests on the *Litchi*-KO mice revealed a greater propensity for exhaustion. Therefore, combining these electrophysiological and behavioral results, *Litchi* depletion likely affects mouse motor performance, such as endurance and maximum strength force. Our electrophysiology data was generated from neurons cultured *in vitro*. Future electrophysiological assessments should focus on *Litchi* KO *in vivo* with an MN reporter to strengthen the evidence for its essential role in MN maturation.

Given that the perturbation of initial spike doublets has been observed in disease models of certain neurological disorders, such as epilepsy, amyotrophic lateral sclerosis (ALS) and aging,^{31–33} the electrophysiological phenotype displayed by our *Litchi*-KO mice mirrors the altered motor behaviors of some human disorders. Several previous studies have revealed that lncRNA knockout models only exhibit prominent phenotypes after experiencing stress,²⁵ which might explain in part why we observed a stronger defect in neurite complexity and a greater reduction in MN function upon *Litchi* knockout under *in vitro* differentiation conditions compared to the *in vivo* knockout embryos. Interestingly, the compromised MN activity in the *Litchi*-KO mice became more prominent upon aging. Notably, *Litchi* overexpression in neurons extended neurite outgrowth, implying that this could be a potential treatment avenue against neuronal disorders related to dendritic and axonal degeneration. Thus, we are currently testing if *Litchi* expression is changed upon spinal cord injury and/or in MN neurodegenerative disease such as ALS, and if *Litchi* overexpression might be adopted as a new therapeutic application. Therefore, our study unveils a previously underestimated dimension of lncRNAs in intricately guiding the process of MN maturation and robust function. The intricate regulatory activity of *Litchi* in this study highlights the wider importance of lncRNAs in the landscape of neural maturation. This significant revelation paves the way for further promising studies on lncRNAs in terms of how they contribute to neuronal function and why they go awry in neurodegenerative diseases.

Limitations of the study

In this investigation, we have diligently crafted a mouse model designed to selectively eliminate the lncRNA *Litchi* while preserving its host gene. This approach provides a proof-of-concept illustrating how a single neuronal lncRNA, when removed, influences the maturation and electrophysiological resilience of spinal MNs. As an expanding repertoire of lncRNAs exclusive to MNs is unveiled, our study aims to shed light on the elusive functions of these transcripts within the intricate circuits of the adult nervous system. However, our current understanding of how *Litchi* mechanistically regulates voltage-gated channels and other genes governing adult neuronal homeostasis remains incomplete. Future investigations aimed at identifying the *Litchi* interactome have the potential to clarify unresolved aspects of this issue. It is essential to acknowledge that our electrophysiology data was derived from neurons cultured *in vitro*. To substantiate evidence of *Litchi*'s indispensable role in MN maturation, future electrophysiological assessments should prioritize *Litchi* knockout *in vivo* for a more robust investigation of its functional significance.

STAR★METHODS

Detailed methods are provided in the online version of this paper and include the following:

- KEY RESOURCES TABLE
- RESOURCE AVAILABILITY
 - Lead contact
 - Materials availability
 - Data and code availability
- EXPERIMENTAL MODEL AND STUDY PARTICIPANT DETAILS
 - Mouse breeding and maintenance
 - Mouse ESC culture
 - Mouse primary culture
- METHOD DETAILS

- Mouse ESC differentiation
- CRISPR/Cas9 gene editing of mouse ESCs and mouse model
- Mouse tissue collection
- Quantitative real-time PCR
- Immunostaining
- Quantification of neurite outgrowth
- *In situ* hybridization
- RNAscope
- Electrophysiology
- Microarray
- Open field test
- Rotarod test
- Grip strength test
- **QUANTIFICATION AND STATISTICAL ANALYSIS**

SUPPLEMENTAL INFORMATION

Supplemental information can be found online at <https://doi.org/10.1016/j.isci.2024.109207>.

ACKNOWLEDGMENTS

We thank the Transgenics Core Facility of IMB Academia Sinica that generated the *Litchi*-KO mice. We also acknowledge the NPAS Neuro-electrophysiology Core in Academia Sinica and the Taiwan Mouse Clinic for their help with patched clamp experiments and mouse behavior assays. This work is funded by Academia Sinica (AS-BRPT-113-01 and AS-GCP-113-L02), the National Science and Technology Council (112-2326-B-001-001), and the National Health Research Institutes (NHRI-EX113-11330NI).

AUTHOR CONTRIBUTIONS

Conceptualization, J.-A.C. and H.-C.H.; methodology, H.-C.H., S.-P.H., F.-Y.H., and M.C., software and formal analysis, H.-C.H. and S.-P.H.; investigation, H.-C.H., S.-P.H., F.-Y.H., and J.-A.C.; writing – original draft, J.-A.C. and H.-C.H.; writing – review and editing, J.-A.C. and H.-C.H.; funding acquisition, J.-A.C.; supervision, J.-A.C.

DECLARATION OF INTERESTS

The authors declare no potential conflicts of interest for this work.

Received: September 27, 2023

Revised: December 8, 2023

Accepted: February 7, 2024

Published: February 10, 2024

REFERENCES

1. Vance, K.W., and Ponting, C.P. (2014). Transcriptional regulatory functions of nuclear long noncoding RNAs. *Trends Genet.* 30, 348–355. <https://doi.org/10.1016/j.tig.2014.06.001>.
2. Carlevaro-Fita, J., and Johnson, R. (2019). Global Positioning System: Understanding Long Noncoding RNAs through Subcellular Localization. *Mol. Cell* 73, 869–883. <https://doi.org/10.1016/j.molcel.2019.02.008>.
3. Mattick, J.S., Amaral, P.P., Carninci, P., Carpenter, S., Chang, H.Y., Chen, L.L., Chen, R., Dean, C., Dinger, M.E., Fitzgerald, K.A., et al. (2023). Long non-coding RNAs: definitions, functions, challenges and recommendations. *Nat. Rev. Mol. Cell Biol.* 24, 430–447. <https://doi.org/10.1038/s41580-022-00566-8>.
4. Cajigas, I., Leib, D.E., Cochrane, J., Luo, H., Swyter, K.R., Chen, S., Clark, B.S., Thompson, J., Yates, J.R., 3rd, Kingston, R.E., and Kohtz, J.D. (2015). Evi2 lncRNA/BRG1/DLX1 interactions reveal RNA-dependent inhibition of chromatin remodeling. *Development* 142, 2641–2652. <https://doi.org/10.1242/dev.126318>.
5. Huarte, M., Guttman, M., Feldser, D., Garber, M., Koziol, M.J., Kenzelmann-Broz, D., Khalil, A.M., Zuk, O., Amit, I., Rabani, M., et al. (2010). A large intergenic noncoding RNA induced by p53 mediates global gene repression in the p53 response. *Cell* 142, 409–419. <https://doi.org/10.1016/j.cell.2010.06.040>.
6. Rinn, J.L., Kertesz, M., Wang, J.K., Squazzo, S.L., Xu, X., Bruggmann, S.A., Goodnough, L.H., Helms, J.A., Farnham, P.J., Segal, E., and Chang, H.Y. (2007). Functional demarcation of active and silent chromatin domains in human HOX loci by noncoding RNAs. *Cell* 129, 1311–1323. <https://doi.org/10.1016/j.cell.2007.05.022>.
7. Yen, Y.P., Hsieh, W.F., Tsai, Y.Y., Lu, Y.L., Liau, E.S., Hsu, H.C., Chen, Y.C., Liu, T.C., Chang, M., Li, J., et al. (2018). Dlk1-Dio3 locus-derived lncRNAs perpetuate postmitotic motor neuron cell fate and subtype identity. *Elife* 7, e38080. <https://doi.org/10.7554/eLife.38080>.
8. Noh, J.H., Kim, K.M., McClusky, W.G., Abdelmohsen, K., and Gorospe, M. (2018). Cytoplasmic functions of long noncoding RNAs. *Wiley Interdiscip. Rev. RNA* 9, e1471. <https://doi.org/10.1002/wrna.1471>.
9. Chen, T.H., and Chen, J.A. (2019). Multifaceted roles of microRNAs: From motor neuron generation in embryos to degeneration in spinal muscular atrophy. *Elife* 8, e50848. <https://doi.org/10.7554/eLife.50848>.
10. Chen, K.W., and Chen, J.A. (2020). Functional Roles of Long Non-coding RNAs in Motor Neuron Development and Disease. *J. Biomed. Sci.* 27, 38. <https://doi.org/10.1186/s12929-020-00628-z>.
11. Statello, L., Guo, C.J., Chen, L.L., and Huarte, M. (2021). Gene regulation by long non-coding RNAs and its biological functions.

- Nat. Rev. Mol. Cell Biol. 22, 96–118. <https://doi.org/10.1038/s41580-020-00315-9>.
12. Briggs, J.A., Wolvetang, E.J., Mattick, J.S., Rinn, J.L., and Barry, G. (2015). Mechanisms of Long Non-coding RNAs in Mammalian Nervous System Development, Plasticity, Disease, and Evolution. *Neuron* 88, 861–877. <https://doi.org/10.1016/j.neuron.2015.09.045>.
 13. Sagner, A., and Briscoe, J. (2019). Establishing neuronal diversity in the spinal cord: a time and a place. *Development* 146, dev182154. <https://doi.org/10.1242/dev.182154>.
 14. Philippidou, P., and Dasen, J.S. (2013). Hox genes: choreographers in neural development, architects of circuit organization. *Neuron* 80, 12–34. <https://doi.org/10.1016/j.neuron.2013.09.020>.
 15. Jessell, T.M. (2000). Neuronal specification in the spinal cord: inductive signals and transcriptional codes. *Nat. Rev. Genet.* 1, 20–29.
 16. Alaynick, W.A., Jessell, T.M., and Pfaff, S.L. (2011). SnapShot: spinal cord development. *Cell* 146, 178–178.e1.
 17. Briscoe, J., Pierani, A., Jessell, T.M., and Ericson, J. (2000). A homeodomain protein code specifies progenitor cell identity and neuronal fate in the ventral neural tube. *Cell* 101, 435–445.
 18. Liao, E.S., Jin, S., Chen, Y.C., Liu, W.S., Calon, M., Nedelec, S., Nie, Q., and Chen, J.A. (2023). Single-cell transcriptomic analysis reveals diversity within mammalian spinal motor neurons. *Nat. Commun.* 14, 46. <https://doi.org/10.1038/s41467-022-35574-x>.
 19. Carvelli, A., Setti, A., Desideri, F., Galfrè, S.G., Biscarini, S., Santini, T., Colantoni, A., Peruzzi, G., Marzi, M.J., Capauto, D., et al. (2022). A multifunctional locus controls motor neuron differentiation through short and long noncoding RNAs. *EMBO J.* 41, e108918. <https://doi.org/10.15252/embj.2021108918>.
 20. Biscarini, S., Capauto, D., Peruzzi, G., Lu, L., Colantoni, A., Santini, T., Shneider, N.A., Caffarelli, E., Laneve, P., and Bozzoni, I. (2018). Characterization of the lncRNA transcriptome in mESC-derived motor neurons: Implications for FUS-ALS. *Stem Cell Res.* 27, 172–179. <https://doi.org/10.1016/j.scr.2018.01.037>.
 21. Li, C.J., Liao, E.S., Lee, Y.H., Huang, Y.Z., Liu, Z., Willems, A., Garside, V., McGlenn, E., Chen, J.A., and Hong, T. (2021). MicroRNA governs bistable cell differentiation and lineage segregation via a noncanonical feedback. *Mol. Syst. Biol.* 17, e9945. <https://doi.org/10.15252/msb.20209945>.
 22. Delile, J., Rayon, T., Melchionda, M., Edwards, A., Briscoe, J., and Sagner, A. (2019). Single cell transcriptomics reveals spatial and temporal dynamics of gene expression in the developing mouse spinal cord. *Development* 146, dev173807.
 23. Tung, Y.T., Peng, K.C., Chen, Y.C., Yen, Y.P., Chang, M., Thams, S., and Chen, J.A. (2019). Mir-17~92 Confers Motor Neuron Subtype Differential Resistance to ALS-Associated Degeneration. *Cell Stem Cell* 25, 193–209.e7. <https://doi.org/10.1016/j.stem.2019.04.016>.
 24. Blum, J.A., Klemm, S., Shadrach, J.L., Guttenplan, K.A., Nakayama, L., Kathiria, A., Hoang, P.T., Gautier, O., Kaltschmidt, J.A., Greenleaf, W.J., and Gitler, A.D. (2021). Single-cell transcriptomic analysis of the adult mouse spinal cord reveals molecular diversity of autonomic and skeletal motor neurons. *Nat. Neurosci.* 24, 572–583. <https://doi.org/10.1038/s41593-020-00795-0>.
 25. He, D., Wang, J., Lu, Y., Deng, Y., Zhao, C., Xu, L., Chen, Y., Hu, Y.-C., Zhou, W., and Lu, Q.R. (2017). lncRNA functional networks in oligodendrocytes reveal stage-specific myelination control by an lncOL1/Suz12 complex in the CNS. *Neuron* 93, 362–378.
 26. Turner, R.W., Maler, L., Deerinck, T., Levinson, S.R., and Ellisman, M.H. (1994). TTX-sensitive dendritic sodium channels underlie oscillatory discharge in a vertebrate sensory neuron. *J. Neurosci.* 14, 6453–6471.
 27. Driesang, R.B., and Pape, H.-C. (2000). Spike doublets in neurons of the lateral amygdala: mechanisms and contribution to rhythmic activity. *Neuroreport* 11, 1703–1708.
 28. Whittington, M.A., Traub, R.D., Faulkner, H.J., Stanford, I.M., and Jefferys, J.G. (1997). Recurrent excitatory postsynaptic potentials induced by synchronized fast cortical oscillations. *Proc. Natl. Acad. Sci. USA* 94, 12198–12203.
 29. Nishimoto, Y., Nakagawa, S., Hirose, T., Okano, H., Takao, M., Shibata, S., Suyama, S., Kuwako, K.-I., Imai, T., Murayama, S., et al. (2013). The long non-coding RNA nuclear-enriched abundant transcript 1_2 induces paraspeckle formation in the motor neuron during the early phase of amyotrophic lateral sclerosis. *Mol. Brain* 6, 31.
 30. Kirkwood, P.A., and Munson, J.B. (1996). The incidence of initial doublets in the discharges of motoneurons of two different inspiratory muscles in the cat. *J. Physiol.* 493, 577–587.
 31. Cox, G.A., Lutz, C.M., Yang, C.-L., Biemesderfer, D., Bronson, R.T., Fu, A., Aronson, P.S., Noebels, J.L., and Frankel, W.N. (1997). Sodium/hydrogen exchanger gene defect in slow-wave epilepsy mutant mice. *Cell* 91, 139–148.
 32. Kleine, B.U., Stegeman, D.F., Schelhaas, H.J., and Zwarts, M.J. (2008). Firing pattern of fasciculations in ALS: evidence for axonal and neuronal origin. *Neurology* 70, 353–359.
 33. Chang, Y.-M., Rosene, D.L., Killiany, R.J., Mangiamele, L.A., and Luebke, J.I. (2005). Increased action potential firing rates of layer 2/3 pyramidal cells in the prefrontal cortex are significantly related to cognitive performance in aged monkeys. *Cerebr. Cortex* 15, 409–418.
 34. Jacko, M., Weyn-Vanhenhenryck, S.M., Smerdon, J.W., Yan, R., Feng, H., Williams, D.J., Pai, J., Xu, K., Wichterle, H., and Zhang, C. (2018). Rbfox Splicing Factors Promote Neuronal Maturation and Axon Initial Segment Assembly. *Neuron* 97, 853–868.e6. <https://doi.org/10.1016/j.neuron.2018.01.020>.
 35. Wichterle, H., Lieberam, I., Porter, J.A., and Jessell, T.M. (2002). Directed differentiation of embryonic stem cells into motor neurons. *Cell* 110, 385. [https://doi.org/10.1016/s0092-8674\(02\)00835-8](https://doi.org/10.1016/s0092-8674(02)00835-8).
 36. Cong, L., Ran, F.A., Cox, D., Lin, S., Barretto, R., Habib, N., Hsu, P.D., Wu, X., Jiang, W., Marraffini, L.A., and Zhang, F. (2013). Multiplex genome engineering using CRISPR/Cas systems. *Science*. 339, 819. <https://doi.org/10.1126/science.1231143>.
 37. Iacovino, M., Bosnakovski, D., Fey, H., Rux, D., Bajwa, G., Mahen, E., Mitanoska, A., Xu, Z., and Kyba, M. (2011). Inducible cassette exchange: a rapid and efficient system enabling conditional gene expression in embryonic stem and primary cells. *Stem Cell* 29, 1580–1588. <https://doi.org/10.1002/stem.715>.
 38. Schindelin, J., Arganda-Carreras, I., Frise, E., Kaynig, V., Longair, M., Pietzsch, T., Preibisch, S., Rueden, C., Saalfeld, S., Schmid, B., et al. (2012). Fiji: an open-source platform for biological-image analysis. *Nat. Methods* 9, 676. <https://doi.org/10.1038/nmeth.2019>.

STAR★METHODS

KEY RESOURCES TABLE

REAGENT or RESOURCE	SOURCE	IDENTIFIER
Antibodies		
Goat polyclonal anti-Choline Acetyltransferase	Sigma-Aldrich	Cat# AB144P; RRID: AB_2079751
Sheep polyclonal anti-Green Fluorescent Protein	BIO-RAD	Cat# 4745-1051; RRID: AB_619712
Rabbit polyclonal anti-Olig-2	Sigma-Aldrich	Cat# AB9610; RRID: AB_570666
Guinea pig anti-Hb9 (Mnx1)	H. Wichterle (Columbia, New York)	N/A
Mouse monoclonal anti-islet1/anti-islet2 (39.4D5)	DSHB	Cat# 39.4D5; RRID: AB_2314683
Rabbit polyclonal anti-Microtubule-Associated Protein 2	Sigma-Aldrich	Cat# AB5622; RRID: AB_91939
Mouse monoclonal anti-Tau-1 (clone PC1C6)	Sigma-Aldrich	Cat# MAB3420; RRID: AB_94855
Rabbit polyclonal anti-LHX3/LIM	Abcam	Cat# ab14555; RRID: AB_301332
Rabbit polyclonal anti-FOXP1	Abcam	Cat# ab16645; RRID: AB_732428
Mouse monoclonal anti-islet1 (39.3F7)	DSHB	Cat# 39.3F7; RRID: AB_1157901
Biological samples		
Mouse embryonic bodies (ESC-derived MNs)	This paper	N/A
Mouse ESC-derived MNs, dissociated from embryonic bodies	This paper	N/A
Mouse spinal cord cryosections, embryonic	This paper	N/A
Mouse cerebral cryosections, embryonic	This paper	N/A
Mouse spinal cord primary cells	This paper	N/A
Chemicals, peptides, and recombinant proteins		
ESGRO® Recombinant Mouse LIF Protein	Sigma-Aldrich	Cat# ESG1107
Retinoid acid	Millipore	Cat# 554720; CAS: 302-79-4
Smoothened Agonist	Sigma-Aldrich	Cat# 566660; CAS: 364590-63-6
rat GDNF	Peptotech	Cat# 450-51
Deposited data		
Raw and analyzed data	This paper	GSE248380
Next Generation Sequencing Facilitates Quantitative Analysis of ES, pMN, MN, and IN Transcriptomes.	Yen et al. ⁷	GSE114285
Single-cell RNA-seq of mouse developing spinal cord	Delile et al. ²²	E-MTAB-7320
Single-cell transcriptomic analysis unveils the diversity within mammalian spinal motor neurons	Liau et al. ¹⁸	GSE183759
Single-cell transcriptomic analysis of the adult mouse spinal cord reveals fundamental molecular diversity of autonomic and skeletal motor neurons	Blum et al. ²⁴	GSE161621
Experimental models: Cell lines		
Mouse: ES cells: Mnx1::GFP	H. Wichterle (Columbia, New York)	Wichterle et al. ³⁵
Mouse: ES cells: <i>Litchi</i> KO: Mnx1::GFP; <i>Gm2990</i> ^{-/-}	This paper	N/A
Mouse: ES cells: <i>Tet-ON Litchi</i>	This paper	N/A
Mouse: primary fibroblasts, embryonic	This paper	N/A
Mouse: primary cortical astrocytes, embryonic	This paper	N/A
Mouse: primary spinal cord cells, embryonic	This paper	N/A

(Continued on next page)

Continued

REAGENT or RESOURCE	SOURCE	IDENTIFIER
Experimental models: Organisms/strains		
Mouse: <i>Litchi</i> KO: <i>Gm2990</i> ^{-/-}	This paper	N/A
Mouse: Mnx1::GFP	H. Wichterle (Columbia, New York)	Wichterle et al. ³⁵
Mouse: <i>Litchi</i> KO: Mnx1::GFP; <i>Gm2990</i> ^{-/-}	This paper	N/A
Oligonucleotides		
See Table S2 for oligonucleotide list used for quantitative RT-PCR	This paper	N/A
See Table S3 for sgRNA sequence list used in this work	This paper	N/A
See Table S4 for oligonucleotide list used for genotyping	This paper	N/A
See Table S5 for probe list of <i>in situ</i> hybridization and RNAscope	This paper	N/A
Recombinant DNA		
pX330-U6-Chimeric_BB-CBh-hSpCas9	Cong et al. ³⁶	Cong et al. ³⁶ ; RRID: Addgene_42230
p2Loxa	Iacovino et al. ³⁷	Iacovino et al. ³⁷ ; RRID: Addgene_34635
Software and algorithms		
Fiji (ImageJ)	NIH	Schindelin et al. ³⁸ ; RRID: SCR_002285
ZEN	Carl Zeiss	RRID: SCR_013672
MetaXpress	Molecular Devices	RRID: SCR_016654
Prism 9	GraphPad	RRID: SCR_002798
pClamp 10	Molecular Devices	RRID: SCR_011323
RStudio	Posit, PBC	RRID: SCR_000432

RESOURCE AVAILABILITY**Lead contact**

Further information and requests for resources and reagents should be directed to and will be fulfilled by the Lead Contact, Jun-An Chen (jac2210@gate.sinica.edu.tw).

Materials availability

This study did not generate new unique reagents.

Data and code availability

- Data: The microarray data produced in this study can be found in the Gene Expression Omnibus repository under the Accession number GSE248380. These data are publicly accessible as of the publication date. Additionally, the public single-cell RNA sequencing datasets for mouse spinal motor neurons utilized in this study were obtained from GSE114285, [E-MTAB-7320](#), GSE183759, and GSE161621.
- Code: This paper does not report original code.
- Others: Any additional information required concerning the data reported in this paper is available from the [lead contact](#) upon request.

EXPERIMENTAL MODEL AND STUDY PARTICIPANT DETAILS**Mouse breeding and maintenance**

To generate *Litchi*-KO mice with the Mnx1::GFP reporter, mouse ESCs hosting Mnx1::GFP were injected into host mice. Several chimeric mice were born and these were further crossed with C57BL/6J wild-type mice for maintenance. A CRISPR/Cas9 approach was used for *Litchi* deletion (see [Table S3](#) and [Method details](#)). All animals were genotyped by PCR (see [Table S4](#)). We employed an equal number of male and female mice at the same ages and developmental times denoted within figure legends and observed no sex differences in this study. The smallest sample size was used that still provided statistical rigor in accordance with 3Rs principles. No animals were involved in previously unrelated experimental procedures. All of the live animals were maintained in a specific-pathogen-free (SPF) animal facility, approved and overseen by IACUC Academia Sinica (IACUC protocol No. 12-07-389).

Mouse ESC culture

The Mnx1::GFP ESC line was derived from blastocysts by mating a transgenic Mnx1::GFP male mouse with a wildtype female mouse, and the blastocysts were cultured in KES medium [EmbryoMax DMEM (Millipore) containing 1x EmbryoMax MEM Non-essential Amino Acids (Millipore), 1x Nucleosides (Millipore), 2 mM L-Glutamine (Invitrogen), 1% Penicillin/Streptomycin (Invitrogen), 0.00072% 2-mercaptoethanol (Sigma), 0.01% leukemia inhibitory factor (Millipore), 3 μ M GSK3 β inhibitor CHIR99021 (Merck), and 50 μ M PD98059 (Merck)]. The Mnx1::GFP mouse ESC line with *Litchi* KO was generated by CRISPR/Cas9 gene editing of Mnx1::GFP ESCs (see [Method details](#)). To maintain ESCs, cells were cultured on gamma-inactivated mouse primary embryonic fibroblasts with ESC culture medium [15% Fetal Bovine Serum (GIBCO), 1x EmbryoMax MEM Non-essential Amino Acids (Millipore), 1x Nucleosides (Millipore), 2 mM L-Glutamine (Invitrogen), 1% Penicillin/Streptomycin (Invitrogen), 0.00072% 2-mercaptoethanol (Sigma), and 1000 μ L/mL LIF/ESGRO (Chemicon/Millipore) in EmbryoMax DMEM (Millipore)], with culture medium replaced each day.

Mouse primary culture

Mouse spinal cords were dissected from E13.5 Mnx1::GFP or Mnx1::GFP; *Litchi*^{-/-} embryos and dissociated by Accutase for 15 min at 37°C. After dissociation, spinal cord specimens were triturated by pipetting until most of the large pieces had disappeared. Triturated spinal cord cells were rinsed twice with DPBS and filtered through a 40- μ m cell strainer (Falcon). To culture primary spinal neurons, cells were plated onto poly-L-ornithine and laminin-coated 24-well plates (1 \times 10⁶ cells/well) with culture medium [Neurobasal medium (Invitrogen) containing 1x Penicillin/Streptomycin, 1x GlutaMAX (GIBCO), 1x B27 supplement (Invitrogen), 1x N2 supplement (Invitrogen) and 1 ng/mL rat GDNF]. The cells were fixed for immunostaining on Day3 of *in vitro* culture (DIV-3). Primary astrocytes for MN co-culture were harvested from mouse cortex according to the same procedure for embryo dissection with a modified culture protocol.

METHOD DETAILS

Mouse ESC differentiation

Mouse ESCs with the Mnx1::GFP reporter were used for MN differentiation in order to analyze lncRNA expression, as well as deployed for CRISPR/Cas9-mediated gene editing. For MN differentiation, ESCs were dissociated into single cells by using 0.05% Trypsin/EDTA (GIBCO) and cultured with differentiation medium [1:1 Advanced DMEM/F12 (Invitrogen) and Neurobasal Medium (Invitrogen) containing 10% Knockout serum (Invitrogen), 1x Penicillin/Streptomycin (Invitrogen), 2 mM L-Glutamine (Invitrogen), and diluted 2-mercaptoethanol (Sigma)] on 100-mm suspension culture dishes at a density of \sim 1 \times 10⁶ ESCs to form embryoid bodies (EBs). After two days, retinoid acid (RA) and Smoothed agonist (SAG) were added to differentiation medium. On Day5, the culture medium was replaced with fresh differentiation medium without RA and SAG. For MN culture, Day5 EBs were dissociated into single cells by Accutase (Innovative Cell Technologies). The dissociated cells were rinsed once with DPBS and plated onto poly-L-ornithine and laminin-coated four-well plates with MN culture medium [1:1 Advanced DMEM/F12 and Neurobasal Medium with 1x Penicillin/Streptomycin, 2 mM L-Glutamine, 1x B27 supplement (Invitrogen), 1x N2 supplement (Invitrogen) and 1 ng/mL rat GDNF]. For neurite morphology and electrophysiology tests, primary cortical astrocytes were plated onto four-well plates two days before dissociated MNs were plated. MNs were harvested on Day6 and Day10 for immunostaining or whole-cell patch clamping. For interneuron differentiation, only RA was added to differentiation medium, and the EBs were dissociated and plated on Day5 and then harvested on Day6.

CRISPR/Cas9 gene editing of mouse ESCs and mouse model

Wildtype humanized *Streptococcus pyogenes* Cas9 plasmid pX330 (Addgene) was used for CRISPR gene editing. To delete the *Litchi* locus from mouse ESCs, two pairs of single-guide RNAs (sgRNAs) were designed using an online design tool [<http://crispr.mit.edu>] to target the 5' and 3' ends of the *Litchi* first and second exons. The top-scoring sgRNA sequences were selected to generate plasmids for *Litchi* exon deletion from Mnx1::GFP mESCs (see [Table S3](#)). The *Litchi* second exon was deleted first. After generating *Litchi*-exon2^{-/-} ESCs, the ESC line was further subjected to exon-1 deletion. The Transgenic Core Facility of Academia Sinica conducted CRISPR editing on C57BL/6J mice to establish the *Litchi*-KO mouse model. The same pair of sgRNA sequences employed to delete the second exon of *Litchi* from mESCs was used for exon-2 deletion in mice.

Mouse tissue collection

Embryonic spinal cords for *in situ* hybridization, immunostaining and RNAscope were collected from wildtype or *Litchi*-KO mouse embryos. Embryos were fixed overnight in 4% paraformaldehyde and then rinsed twice with phosphate-buffered saline (PBS) to remove any remaining paraformaldehyde. Spinal cord samples for RNAscope were collected at postnatal day (P)2 and P120. Mice were first anaesthetized with Avertin and subjected to perfusion with PBS and 4% paraformaldehyde. After the spinal cord was taken out, it was further fixed overnight in 4% paraformaldehyde. All fixed samples were further infiltrated with 30% sucrose before embedding for cryosectioning. Embedded samples were then sectioned coronally to a thickness of 12 μ m using a LEICA cryosection system (LEICA). To determine expression levels of *Litchi* in the Mnx1::RFP; Foxp1::GFP spinal cord, whole embryonic E13.5 spinal cords were dissected out and subjected to fluorescence-activated cell sorting (FACS) (FACSAria II SORP, BD Biosciences) to separate LMC (Mnx1::RFP^{on}; Foxp1::GFP^{on}), MMC (Mnx1::RFP^{on}; Foxp1::GFP^{off}) and non-MN (Mnx1::RFP^{off}; Foxp1::GFP^{off}) spinal neurons. The separated cells were further lysed using Trizol, followed by RNA extraction using a Trizol protocol.

Quantitative real-time PCR

To establish MN-specific lncRNA temporal gene expression patterns, Mnx1::GFP ESCs were differentiated into spinal MNs and Day4~6 whole EBs RNA was extracted using Trizol (Invitrogen). For the lncRNA specificity test, Day6 EBs were dissociated and subjected to fluorescence-activated cell sorting (FACS) (FACSAria II SORP, BD Biosciences) to separate GFP^{on} and GFP^{off} cells. The separated cells were lysed in Trizol-LS (Invitrogen) and their total RNA was further purified using a Direct-zol RNA miniprep kit (Zymo Research). For the total RNA samples used to determine *Litchi*-KO phenotypes, Day6 Ctrl and *Litchi*-KO EBs underwent FACS before being subjected to RNA purification by using a Direct-zol RNA miniprep/microprep kit. The total RNA (~100 ng) was subjected to reverse transcription using SuperScript™ III (Invitrogen) with random hexamers. To perform qPCR, 2x Sybr Green mixture (Roche) was used, and the reaction and analysis were conducted in a LightCycler480® system (Roche, RRID: SCR_020502). *Gapdh* was used for normalization of all quantification data. A list of primers used for quantitative RT-PCR is shown in [Table S2](#).

Immunostaining

For EB sample preparation, Day4~6 EBs were fixed with 4% paraformaldehyde for 30 min, infiltrated with 30% sucrose, embedded, and then cryosectioned (thickness: 12 µm). For ESC-derived MNs preparation, Day6 and Day10 cells were fixed with 4% paraformaldehyde for 30 min on ice and then rinsed several times with PBS. To perform immunostaining, the slides were first rinsed with 0.5% Triton X-100 for permeabilization. Slides were blocked with 5% FBS and then incubated overnight with primary antibodies (see [key resources table](#)) at 4°C. The next day, the samples were rinsed with PBS and incubated with secondary antibodies. DAPI was used to stain nuclei. A laser scanning confocal microscope (LSM710 or LSM780, Zeiss) was used for image acquisition. Fiji ImageJ was used for image processing and Sholl analysis.

Quantification of neurite outgrowth

For Day6 MN outgrowth quantification, GFP signal was acquired using a High Content Screening system (Molecular Devices), and the resulting images were subjected to MetaXpress® Neurite outgrowth quantification according to the manufacturer's instructions. For Day9 ESC~MNs and DIV-3 primary cell neurite quantification, immunostaining results of Tau-1 and Map2 were acquired by confocal microscopy (LSM710, Zeiss). A single neuron was acquired from each image for subsequent Sholl analysis. A Sholl analysis plugin from Fiji was used to quantify Day9 Map2-positive neurite complexity. For Sholl analysis, the starting radius was set as 10 µm, and step sizes (intervals between radii) were set as 5 and 2 µm for ESC~MNs and primary MNs, respectively. For statistical analysis, two-way ANOVA was used to evaluate neurite complexity between two genotypes (Ctrl and *Litchi* KO) at different distances, and statistical significance of the difference between Ctrl and *Litchi* KO is presented.

In situ hybridization

A FITC-conjugated *Litchi* probe was designed and then synthesized by means of *in vitro* transcription (Roche) and the probe sequence is presented in [Table S5](#). Before performing *in situ* hybridization, the sections were re-fixed by using 4% paraformaldehyde, treated with proteinase K, and then acetylated with acetic anhydride (Sigma-Aldrich). For probe hybridization, the sections were first incubated with hybridization buffer [50% formamide, 5x saline-sodium citrate (SSC), 5x Denhardt's solution, 250 µg/mL yeast RNA, 500 µg/mL salmon sperm DNA, 2% Roche blocking reagent] for at least 3 hours. After incubation, the sections were hybridized overnight with *Litchi* probes (1000 ng/mL in hybridization buffer) at 55°C. The next day, the samples were rinsed several times with SSC and further incubated with antibody blocking solution [1% BMB (1,4-bismaleimidobutane) and 10% fetal bovine serum in maleic acid buffer (MAB; 100 mM maleic acid, 150 mM sodium chloride)] for 1 hour. After blocking, samples were incubated overnight with antibody (FITC, Roche) at 4°C. After antibody hybridization, samples were rinsed several times with MAB buffer and alkalized by alkaline phosphatase buffer (100 mM Tris, 50 mM magnesium chloride, 100 mM sodium chloride, 0.1% Tween-20). NBT/BCIP was used for color development. Samples were acquired by AxioImager Z1 microscopy (Zeiss).

RNAscope

RNAscope™ probes were designed and synthesized by Advanced Cell Diagnostics and generally followed the hybridization procedure of the vendor. In brief, sections were fixed using 4% paraformaldehyde and then treated with hydrogen peroxide and proteinase K. Next, the sections were incubated with RNAscope probes (*Litchi* C2 and *slc18a3* C3 probes, see [Table S5](#)) for 2 hours. After hybridization, sections were incubated with pre-amplifiers, amplifiers and label probes. Labeled probes were visualized using Opal 520 (FP1487001KT) and 570 (FP1488001KT) fluorophores. A laser scanning confocal microscope (LSM710 or LSM780, Zeiss) was used for image acquisition.

Electrophysiology

Sample preparation and recording conditions for electrophysiological analyses were modified from Jacko et al.³⁴ Mnx1::GFP EBs were dissociated into single cells on Day5 and subjected to FACS to separate out the GFP^{on} postmitotic MNs. Sorted MNs were then co-cultured with primary cortical astrocytes on 15-mm glass coverslips at a density of 60 GFP^{on} MNs/mm². On Day6 or Day10, the samples underwent whole-cell patch clamp recording (Zeiss AxioVert AI system, provided by the Neuroelectrophysiology Core of the Neuroscience Program of Academia Sinica). Signals were recorded using pClamp software (Molecular Devices). Patch pipettes were prepared with a pipette puller and filamented capillary glass, and filled with internal solution (131 mM K-gluconate, 20 mM KCl, 10 mM HEPES, 8 mM NaCl, 2 mM EGTA, 2 mM MgATP and 0.3 mM Na₃GTP, pH 7.3 at an osmolality of 310 mOsm). External recording solution (92 mM NaCl, 30 mM NaHCO₃, 25 mM glucose,

20 mM HEPES, 5 mM Na-ascorbate, 2.5 mM KCl, 2 mM thiourea, 3 mM Na-pyruvate, 2 mM CaCl₂, 2 mM MgSO₄ and 1.25 mM NaH₂PO₄, pH 7.3) was applied during the clamp procedure. To establish features of the action potential, rheobase was measured from the first action potential. For this calculation, the amplitude was measured from the threshold potential to the maximum potential. After recording, cells underwent fixation and immunostaining for Chat antibody to re-confirm the cell type of recorded neurons.

Microarray

RNA samples for microarray analysis were harvested from Ctrl or *Litchi*^{-/-} dissociated MNs on Day7 and Day9. Before the samples were applied to microarray analysis, the samples were qualified using a Bioanalyzer 2100 system (Agilent). A One-color Low Input Quick Amp Kit (Agilent) was used for labeling, and the labeled samples were hybridized to a SurePrint G3 Mouse GE microarray. Microarray results were read using an Agilent Scanner (Agilent). For gene ontology analysis of the resulting microarray data, differentially expressed genes were identified according to a fold-change of at least 2 for *Litchi*-KO samples relative to control. GeneSpring software was used to analyze downregulated GO terms at different developmental stages.

Open field test

An arena of area 48 x 48 cm and a height of 35 cm was used as an open field. Before testing, WT or *Litchi*-KO mice aged 1.5 months were transferred in a home cage to the behavioral test room for 1 hour. Then the mice were placed individually in the arena for 60 min to record exploration and motor behaviors. All behaviors were recorded using a live video-tracking system positioned above the arena (Clever System, Reston, VA).

Rotarod test

A commercially available rotarod apparatus (47600 Rota-Rod, Ugo Basile, Italy) with a rotating rod of diameter 5 cm was used for the rotarod assay. Before testing, WT or *Litchi*-KO mice were transferred in a home cage to the behavioral testing room for at least 15 mins. During the training phase, the mice were subjected to three trials at a constant speed of 4 rpm and a 60-sec cut-off time to ensure that all test mice could stay on the rod for the duration of a training trial before undergoing a test phase. After a 30 min pause, the mice were evaluated during the test phase, with the rod accelerating from 4 to 40 rpm with a 300-sec cut-off time in a series of three trials. The best performance from the three trials was used for motor coordination evaluation.

Grip strength test

A grip strength meter (MK-380CM/R, Muromachi Kikai Co, Tokyo, Japan) was used for forelimb grip strength analysis. Before testing, WT or *Litchi*-KO mice were transferred in a home cage to the behavioral testing room for 1 hour and their body weight was determined. Then, the mice were presented to the meter until they grabbed the meter with their forelimbs. In order to test grip force, each mouse was pulled away from the meter until they released both forelimbs from the apparatus and the maximum force of their grip was determined by the meter. Each mouse underwent three trials and the ratio of the average recorded force strength to body weight was used to represent force strength per gram weight.

QUANTIFICATION AND STATISTICAL ANALYSIS

Quantitative data are presented as means \pm SD (standard deviation). Statistical analysis was performed in Graph Pad Prism 9.0 (GraphPad Software). All experiments were performed in parallel with both experimental and control genotypes. Two-tailed t-tests were used to compare two different genotypes (WT and *Litchi* KO). For the time course analyses of *Litchi* expression by RNAscope and Sholl analysis, one-way ANOVA and two-way ANOVA were used to determine significant differences between time points or genotypes, respectively. Asterisks *, ** and *** are used to label statistical significance in all figures with P values < 0.05, < 0.01 and < 0.001, respectively.